Straining of Polyelectrolyte-Stabilized Nanoscale Zero Valent Iron Particles during Transport through Granular Porous Media

Trishikhi Raychoudhury[1,3], Nathalie Tufenkji[2], Subhasis Ghoshal[1,]*

[1]Department of Civil Engineering, McGill University, Montreal, Quebec, Canada H3A 2K6

[2]Department of Chemical Engineering, McGill University, Montreal, Quebec, Canada H3A 2B2

[3]Current Address: Department of Applied Geosciences, Technische Universität Berlin, 10587 Berlin, Germany

* Corresponding author. Tel.: +1-514-398-6867, E-mail address: subhasis.ghoshal@mcgill.ca

Abstract

In this study, the relevance of straining of nano-sized particles of zero valent iron coated with carboxymethyl cellulose (CMC-NZVI) during transport in model subsurface porous media is assessed. Although deposition of polyelectrolyte stabilized-NZVI on granular subsurface media due to physicochemical attachment processes has been reported previously, there is limited knowledge on the significance of the collector (sand) diameter on the deposition and spatial distribution of the retention of such nanoparticles. Experiments were conducted to assess the transport of CMC-NZVI in columns packed with four different-sized sands of mean diameter of 775 µm, 510 µm, 250 µm and 150 µm and at three different particle concentrations of 0.085 gL^{-1}, 0.35 gL^{-1} and 1.70 gL^{-1}. CMC-NZVI effluent concentrations decreased with smaller sand diameters. High CMC-NZVI particle retention near the inlet, particularly for the finer sands was observed, even with a low ionic strength of 0.1 mM for the electrolyte medium. These observations are consistent with particle retention in porous media due to straining and/or wedging. Two colloid transport models, one considering particle retention by physicochemical deposition and detachment of those deposited particles, and the other considering particle retention by straining along with particle deposition and detachment, were fitted to the experimental data. The model accounting for straining shows a better fit, especially to the CMC-NZVI retention data along the length of the column. The straining rate coefficients decreased with larger sand diameters. This study demonstrates that CMC-NZVI particles, despite of their small size (hydrodynamic diameters of 167 to 185 nm and transmission electron microscopy imaged diameters of approximately 85 nm), may be removed by straining during transport, especially through fine granular subsurface media. The tailing effect, observed in the particle breakthrough curves, is attributed to detachment of deposited particles.

Keywords: colloid transport; colloid deposition; nanoparticles; groundwater remediation

1. Introduction

The direct injection of reactive nanoscale zero valent iron (NZVI) particles into aquifers is an emerging technology for *in situ* remediation of groundwater contaminated by chlorinated organic compounds (Mueller et al., 2012; O'Carroll et al., 2012; Zhang, 2003). A number of studies have demonstrated that colloidal stabilization of NZVI particles by coating with polymers or polyelectrolytes is necessary for facilitating particle transport in subsurface porous media (Phenrat et al., 2008; Raychoudhury et al., 2010). Several potentially biodegradable and non-toxic polyelectrolytes have been identified, which when sorbed or bonded to the NZVI particle surface, provide colloidal stabilization by creating significant electrosteric forces that counter the strong inter-particle magnetic attractive forces (Petosa et al., 2010; Phenrat et al., 2008).

The deposition of NZVI particles in subsurface granular porous media is influenced by several factors such as the size and aggregation state of the nanoparticles, the surface chemistry of the nanoparticles, the chemistry of the pore fluid, the fluid velocity (Fatisson et al., 2010; He et al., 2009; Petosa et al., 2010; Phenrat et al., 2009; Raychoudhury et al., 2012). The retention of surface-modified NZVI has been reported to decrease with increasing approach velocities and this is attributed to the significant drag forces at higher velocities that promote detachment of deposited particles (He et al., 2009; Phenrat et al., 2010; Raychoudhury et al., 2010). Significant retention of colloids other than NZVI has been observed, even under unfavourable deposition conditions such as low IS, where there is high electrostatic repulsion between similarly charged colloid and collector surfaces. This observation has been attributed to mechanisms such as straining and wedging of colloids between collector grains and attachment of particles on charge heterogeneities on collector surfaces (Redman et al., 2004; Tufenkji and Elimelech, 2005).

77   There are limited reports on the effects of collector size on NZVI or other nanoparticle

78   transport. The collector (sand) size can have a significant effect on nanoparticle transport through

79   porous media because it influences the surface area available for deposition of colloids as well as

80   the pore size and fluid velocities encountered by the colloids. Decreases in pore size can lead to

81   retention of nanoparticles by straining. To the best of our knowledge, Phenrat et al. (2010) is the

82   only study that has investigated the effects of sand size on polymer stabilized-NZVI transport. In

83   that study a reduction in C/C_0 with increase in sand size was observed, which is contrary to the

84   classical colloid filtration theory that suggests more particle deposition with an increase in the

85   single-collector contact efficiency with decrease in sand size (Tufenkji et al., 2004).

86   Furthermore, the observation does not match with previous studies on the transport of latex

87   colloids in different sized sands (Bradford et al., 2003; Xu et al., 2006).

88   A few studies have suggested that nanoparticles, such as those of hematite, maghemite and

89   maghemite/nickel of diameters in the range of 15-50 nm, and single-walled carbon nanotubes of

90   hydrodynamic diameters of 122 nm can be retained in packed columns of sand or soil due to

91   straining (Hong et al., 2009; Jaisi and Elimelech, 2009). These studies have not assessed the

92   elution and retention of nanoparticles along the column length in a range of sand sizes. The

93   relevance of straining was concluded from observations that the steady-state effluent

94   concentration of those nanoparticles decreased under conditions favourable to aggregation. A

95   more robust approach to assessment of straining requires evaluation of the effects of sand size on

96   particle retention profile along the column length in conjunction with the breakthrough curves

97   (Bradford et al., 2003). Straining of colloids is characterized by significantly higher deposition

98   near the injection point than what can be ascribed to physicochemical deposition, as well as by

99   decreasing effluent concentrations in finer sands.

100   A few recent studies have demonstrated that polymer stabilized-NZVI particles, when

101   injected in the field, were retained within three meters from the point of injection (He et al.,

102   2010; Johnson et al., 2013; Su et al., 2013). It is thus important to understand the various colloid

103   retention mechanisms contributing to the spatial distribution of polymer stabilized-NZVI in

104   granular porous media, and the role of sand size in such retention behaviour.

105   The objectives of this study are to assess the extent of deposition and the spatial patterns of

106   deposition of CMC-NZVI during transport in a packed sand column, and to assess whether

107   straining can be a dominant retention mechanism during transport of CMC-NZVI in subsurface

108   granular media. Column transport experiments were conducted where the CMC-NZVI effluent

109   breakthrough patterns were assessed during CMC-NZVI injection and subsequent flushing with

110   the background electrolyte solution. The size of CMC-NZVI particles in the suspensions injected

111   in the column was stable with time. Following each transport experiment, the packed columns

112   were sectioned and the CMC-NZVI retention profile along the column length was analyzed.

113   Because straining is dependent on pore throat size and thus on sand grain size, four different

114   sand sizes were selected for this study. The application of NZVI for remediation requires its

115   injection into aquifers at concentrations up to several gL^{-1}. Thus, the column experiments were

116   conducted with CMC-NZVI concentrations ranging up to 1.7 gL^{-1}. Two colloid transport models

117   considering 1) particle deposition and detachment of deposited particles, and 2) straining along

118   with deposition and detachment of deposited particles were fitted to the experimental data to

119   evaluate the role of straining in CMC-NZVI retention.

120

121   ## 2. Theoretical Approach

122   Nanoparticle transport in granular porous media is often described by the colloid transport

123   model that accounts for advection, dispersion and deposition of colloids onto collector surfaces

124   (Kuhnen et al., 2000; Tufenkji and Elimelech, 2005). Detachment of deposited particles is also

125   accounted for in certain cases, especially, when the particles are deposited under unfavourable

126   conditions. Detachment is most likely when the torque acting on a deposited particle due to

127   hydrodynamic drag is greater than the torque acting on it due to adhesive forces (Bergendahl and

128   Grasso, 2000; Torkzaban et al., 2007). Our calculations reported elsewhere (Raychoudhury et al.,

129   2012) suggests that applied torque on the deposited CMC-NZVI particles due to hydrodynamic

130   drag is greater than the adhesive torque under these experimental conditions, which makes

131   detachment from the sand surfaces feasible. Particle retention due to straining can be

132   represented by modifications to the colloid transport equations as shown in Equations 1-3

133   (Bradford et al., 2003).

134

135
$$\frac{\partial C}{\partial t} = D\frac{\partial^2 C}{\partial x^2} - v_x \frac{\partial C}{\partial x} - k_{dep}C - k_{str}\psi_{str}C + \frac{\rho k_{det}S_{dep}}{\varepsilon} \tag{1}$$

136
$$\rho\frac{\partial S_{dep}}{\partial t} = \varepsilon k_{dep}C - \rho k_{det}S_{dep} \tag{2}$$

137
$$\rho\frac{\partial S_{str}}{\partial t} = \varepsilon k_{str}\psi_{str}C \tag{3}$$

138

139   where C (ML^{-3}) is the suspended particle mass concentration and varies with the distance x (L)

140   and time t (T). D (L^{2}T^{-1}) is the hydrodynamic dispersion coefficient, v_x (LT^{-1}) is the pore water

141   velocity, ρ (ML^{-3}) is the bulk density of sand, and ε is the porosity of the sand packed column.

142   The particle deposition rate coefficient (k_{dep}) described in Equation 4, is related to the single-

143   collector contact efficiency (η_0) which accounts for particle-sand collisions due to particle

144   diffusion, interception and sedimentation (Yao et al., 1971) and the attachment efficiency (α_{pc})

145   between a particle and a collector.

146    $$k_{dep} = \left[\frac{3(1-\varepsilon)U}{2d_c\varepsilon} \alpha_{pc} \right] \eta_0 \qquad (4)$$

147   where U (LT^{-1}) is the Darcy velocity, d_c (L) is the average grain diameter and η_0 can be

148   calculated using the Tufenkji and Elimelech equation (Tufenkji and Elimelech, 2004).

149   In Equation 1, k_{det} (T^{-1}) is the detachment rate coefficient, k_{str} (T^{-1}) is the straining rate

150   coefficient, and ψ_{str} is the dimensionless colloid straining function defined by $\psi_{str} = (\frac{d_c}{d_c + x})^\beta$ as

151   described in Bradford et al. (2003). The parameter β describes the spatial distribution of strained

152   particles along the length of the column and S_{dep} (MM^{-1}) is the deposited mass and S_{str} (MM^{-1}) is

153   the strained mass of particles per unit mass of sand.

154   In this study, the experimental data was analyzed using two colloid transport models.

155   Model 1 accounts for colloid transport due to 1-dimensional advection, dispersion, particle

156   deposition and detachment. The solid phase retention of CMC-NZVI resulting from particle

157   deposition (and detachment) was evaluated by considering Equation 2 which neglects straining

158   of particles (i.e., k_{str} (T^{-1}) was set to zero in Equations 1 and 3). In Model 2, the solid phase

159   retention due to deposition and detachment and straining was calculated using Equations 2 and 3,

160   respectively. The coefficients k_{dep}, k_{det}, and k_{str} were simultaneously fitted to the experimentally

161   determined CMC-NZVI breakthrough curves and retention profiles. The Marquardt algorithm

162   for nonlinear least squares optimization was used to determine the best fit parameters for

163   attachment, detachment and straining (Marquardt, 1963). The sum of squares of residuals

164   between experimental data and model calculations for the relative effluent concentration and the

165 solid phase deposition concentration were minimized simultaneously to obtain the least-squares

166 estimates of the parameters.

167

3. Materials and Methods

169   All chemicals were reagent grade and all solutions were prepared using Milli-Q-UV Plus

170 Ultrapure water (Millipore, MA, USA).

171

3.1 Synthesis and Characterization of CMC-NZVI:

173   The CMC-NZVI preparation method was adapted from (He and Zhao, 2007). Briefly, an

174 aqueous solution of 0.065M ferrous sulphate heptahydrate ($FeSO_4 \cdot 7H_2O$, AlfaAesar, purity

175 greater than 99%) was added to 5 gL^{-1} of CMC (90K, Sigma-Aldrich) solution prepared in

176 deionised (DI) water and mixed thoroughly for 30 minutes and then the solution was reduced by

177 the drop-wise addition of sodium borohydride solution ($NaBH_4$, Sigma-Aldrich) under N_2

178 atmosphere as described in a prior study. The mixture was then dried overnight under N_2 and

179 stored.

180   CMC-NZVI suspensions having three different concentrations (0.085, 0.35 and 1.7 $gFeL^{-1}$)

181 were prepared in 0.1 mM $NaHCO_3$ by sonicating with a 40 kHz ultrasonic cleaner (Cole-Palmer

182 8891) for 10 min to ensure homogeneity of the suspensions and then the suspensions were stirred

183 for 90 min.

184   Particles sizes were assessed at different time points to ensure that 90 min was sufficient to

185 attain stable particle sizes. The mean hydrodynamic diameter was determined by nanoparticle

186 tracking analysis (NTA, NanoSight LM10). Stock suspension of CMC-NZVI of three different

187 concentrations (0.085, 0.35 and 1.7 $gFeL^{-1}$) in 0.1 mM $NaHCO_3$ was filled in a vial under N_2

188   atmosphere to zero headspace. Samples of these suspensions were withdrawn after 90 min and

189   were diluted to 5 mgL^{-1} under an N$_2$ atmosphere immediately prior to NTA measurement as

190   described elsewhere (Raychoudhury et al., 2012).

191

192   **3.2 Packed column experiments:**

193   A glass column (Konets Chromoflex) of 1 cm i.d. and packed bed length of 9 cm was used.

194   A nylon mesh (100 μm) was placed at the bottom of the packed column to prevent sand grains

195   from being displaced into the end adapters. Two batches of silica sand (Unimin Corp, WI,

196   USA), Unimin 4020 and Unimin 2030, were acid washed with 12 N concentrated HCl, rinsed

197   with DI water and oven-dried for 3 hours at 550°C. The washed sands were sieved using nylon

198   mesh and the average size of the sand grains was determined. The sample labelled as F2025

199   passed through an 850 μm sieve (F20) and was retained on a 700 μm (F25) sieve, and its average

200   particle diameter was 775 μm. Similarly, the F3040, F5070, and F70140 sample nomenclature

201   refers to the sieve sizes used, and the average diameters for these samples were 510 μm, 250 μm

202   and 150 μm, respectively. Details of sand sizes and other properties are given in Tables 1 and 2.

203   The column was dry-packed with sand and vibrated intermittently to ensure uniform

204   packing and then saturated with CO$_2$ to ensure removal of air bubbles. The column was

205   conditioned prior to the experiment as described elsewhere (Raychoudhury et al., 2012).

206   A 20 mgL^{-1} KNO$_3$ solution was injected at the same flow rate through all four types of

207   sand packed columns to determine the hydrodynamic dispersion coefficient (D). The porosity (ε)

208   and the value of D, for the columns containing the different sands are presented in Table 1.

209   The influent CMC-NZVI suspensions were prepared at different particle concentrations of

210   0.085, 0.35 and 1.7 gFeL^{-1} in 0.1 mM NaHCO$_3$ as described earlier and pumped downwards at a

211   velocity of 0.445 cm min^{-1} using a syringe pump. The particle suspension pH was 7.4±0.4.

212 Settling of the CMC-NZVI in the syringe was prevented by internal stirring. CMC-NZVI was

213 injected for 2.1 pore volumes (PVs) for the three finer sized sands (510-150μm) and 1.8 PVs for

214 the coarser sand of 775 μm diameter (F2025). Thereafter, several PVs of electrolyte were

215 flushed from the top of the column at the same flow rate as CMC-NZVI injection. All

216 experiments were conducted under N_2 atmosphere and the entire duration of each of the

217 experiments was less than three hours. Therefore oxidation and associated changes to the NZVI

218 size and surfaces during the experiments can be ignored. At the end of the transport experiment,

219 the packed bed was dissected to obtain the mass of iron distributed along the column length.

220 During the sectioning process, care was taken to not disturb the column to avoid displacement of

221 CMC-NZVI from the sand grain surfaces. The sectioned sand samples were digested in an HCl

222 (30% v/v)-HNO_3 (5% v/v) mixture for 48 hours such that the deposited iron particles on the sand

223 were dissolved in the solution. The collected samples were analyzed for total iron as mentioned

224 below. The sand samples were washed with DI water and oven-dried for 24 hours to obtain the

225 dry weight of each segment of the sand bed. The total iron concentration in the samples was

226 analyzed using flame atomic absorption spectrometry (Perkin Elmer 3110) at a wavelength of

227 249.7 nm. All experiments were conducted in duplicate and the average of replicate experiments

228 is reported.

229

230 **4   Results and Discussion**

231 **4.1 Transport of CMC-NZVI at Different Concentrations through Coarse and Fine Sands**

232   The particle hydrodynamic diameters after 90 min of mixing, d_p, for the three CMC-NZVI

233 suspensions of 0.085 gL^{-1}, 0.35 gL^{-1} and 1.70 gL^{-1} concentrations, as measured by NTA were

234 167±64, 183±87 and 185±86 nm, respectively. The mean diameter of the NZVI particles from

235 TEM analyses of CMC-NZVI suspensions after 90 min of mixing was in the range of 85±15 nm.

236 Thus, the zero valent iron particles in this study are referred to as nanoparticles. The details of

237 the TEM analyses are given elsewhere (Raychoudhury et al., 2010). For the pre grafted CMC-

238 NZVI used in this study, the CMC is strongly bound with NZVI, which produces more stable

239 particles compared to CMC-NZVI prepared by coating CMC on NZVI particles (post grafted),

240 which results in weaker binding of CMC to the NZVI (Cirtiu et al., 2011). The CMC-NZVI

241 suspension was polydisperse with particle diameters distributed within a size range of 40-450 nm

242 for 0.085 gL^{-1} CMC-NZVI and 40-600 nm for the two higher concentrations (Figure S3,

243 Supporting information). The proportion of larger aggregates (400-600 nm) in the two more

244 concentrated CMC-NZVI suspensions were less than 0.2 % on a number basis (Figure S3), and

245 also accounted for a negligible mass fraction.

246   CMC-NZVI transport experiments were conducted using columns packed with clean sand

247 having four different mean grain diameters (150 μm, 250 μm, 510 μm and 775 μm) at three

248 different CMC-NZVI influent concentrations of 0.085 gL^{-1}, 0.35 gL^{-1} and 1.70 gL^{-1}, in a solution

249 of 0.1 mM $NaHCO_3$. Figure 1 shows the breakthrough curves (BTCs) and retention profiles of

250 the solid-phase associated CMC-NZVI for a series of four column experiments conducted with

251 0.085 $gFeL^{-1}$ nanoparticle suspensions using four different-sized sands. Similar results were

252 obtained with the 0.35 and 1.70 gL^{-1} CMC-NZVI suspensions and are shown in Figures S1 and

253 S2 in Supplementary data.

254   Figure 1a demonstrates that for the coarsest sand (775 μm) there was near complete

255 breakthrough of the 0.085 gL^{-1} CMC-NZVI suspension with a relative effluent concentration

256 (C/C_0) of 0.95 at 2 PVs. Furthermore, with decreasing average diameter of the sand, the

257 breakthrough value of C/C_0 decreased, indicating greater CMC–NZVI retention. The C/C_0

258 decreased from 0.84 for the 510 μm diameter sand to 0.57 for the 250 μm diameter sand and to

259 0.55 for the 150 μm sand (Table 2). Phenrat et al. (2010) have evaluated the breakthrough

260 patterns of polyelectrolyte modified-NZVI through different sized sand and observed a higher

261 elution (C/C_0) with 99 μm diameter sand compared to coarser sands (300 or 880 μm diameter).

262 Those authors have explained such deposition patterns on the basis of higher pore velocities in

263 the finer sands. According to those authors the higher fluid shear stress acting on aggregates

264 deposited in the finer sands result in breakup or disaggregation of deposited aggregates, leading

265 to higher elution compared to that in coarser sands. In our study, the CMC-NZVI was stabilized

266 for 90 min with particle size range of 45-200 nm (TEM size) before injecting in the column.

267 CMC-NZVI particles in the effluents collected at the end of the injection period had similar size

268 range of 50-200 nm (TEM size), suggesting breakup of aggregates is not significant for pre-

269 grafted CMC-NZVI particles used in this study. This is likely because pre-grafted CMC-NZVI

270 did not produce larger, loose aggregates compared to the post-grafted CMC-NZVI .

271   Figure 1b (and Figures S1b, S2b in Supplementary data) suggests that retention of CMC-

272 NZVI particles at the column inlet increases as the sand size decreases for all three CMC-NZVI

273 influent concentrations. Tailing of the BTCs with continued electrolyte flushing beyond 3 PVs

274 was observed for all cases except with the coarsest sand receiving lowest CMC-NZVI

275 concentration. The tailing is attributable to particle detachment from the sand surface (Li et al.,

276 2005; Tong et al., 2005a). The mass of CMC-NZVI (measured as total Fe) retained in the

277 column as determined from the sectioning data and the mass of CMC-NZVI eluted based on the

278 BTCs were used to evaluate the mass balances of Fe. The overall mass balances of total CMC-

279 NZVI injected ranged between 87-99 % for the various experimental conditions, and are

280 presented as $M_{balance}$ in Table 2.

281   Transport experiments conducted at different CMC-NZVI concentrations showed that

282   normalized effluent concentrations did not vary significantly with changes in influent

283   concentration in the range of 0.085-1.70 gL^{-1} (Figure 1 and Figures S1- S2 in Supplementary

284   data). Phenrat et al. (2009) characterized the transport of polyelectrolyte-coated hematite and

285   NZVI particles. In their study, there was no significant effect of particle concentration on the

286   transport of PSS-coated hematite nanoparticles in the concentration range of 30 mgL^{-1} to 6 gL^{-1}

287   or for PSS-NZVI in the concentration range of 1-6 gL^{-1}. Several studies have reported an effect

288   of concentration on retention of other colloids. For example, Bradford and Bettahar (2006)

289   conducted column transport experiments with micron-sized polystyrene latex particles, and

290   showed that the C/C_0 increased with influent concentration. The existence of hindered straining

291   (liberation) at high colloid concentrations resulted in a higher steady-state C/C_0 value with

292   increasing influent particle concentrations (Bradford and Bettahar, 2006). Kuhnen et al. (2000)

293   found that with an increase in influent iron oxide particle concentrations, a higher C/C_0 was

294   obtained due to blocking of the collector surface. However, our results showed that the

295   normalized effluent particle concentration only varies slightly (less than 10%) with changes in

296   influent concentration suggesting that blocking of collector grain surfaces or hindered straining

297   did not play a significant role in this study.

298   As discussed earlier, the reasons for increased CMC-NZVI retention with decreasing sand

299   size could be: a) change in single-collector contact efficiency with average sand grain size (e.g.,

300   η_0 increases ~2.7 fold, from 0.0173 to 0.0473, as the sand size decreases from 775 μm to 150

301   μm); b) straining and/or wedging at small pores or grain-to-grain contact points; and c) reduced

302   deposition on coarser sands due to blocking. Finer sands have larger specific surface area

303   available for deposition compared to coarser sands, and thus blocking is less likely in finer sands

304   compared to coarser sands. In our study, the sand surface coverage by retained particles were

305   calculated according to methods described elsewhere (Torkzaban et al., 2010), and the fraction of

306   collector surface covered by CMC-NZVI is quite low (in the range of 10^{-5}-10^{-4}) for the different

307   sands. In addition, column experiments conducted at different concentrations suggest that

308   blocking of the collector surfaces is not relevant because there is little variation in relative

309   effluent concentrations with increasing influent concentrations. Thus, in the following section the

310   relevance of the single-collector contact efficiency during transport through sand packed

311   columns is discussed. In addition, detachment of deposited particles was also incorporated in

312   both models to address the tailing observed in the BTCs.

313

314   **4.2 Model 1: Particle Deposition on Sand Surfaces**

315   The experimental data for the BTCs and mass retention profiles along the column length

316   were compared to results calculated using Model 1, which represents CMC-NZVI retention by

317   deposition on collector surfaces and detachment of deposited particles, without consideration of

318   straining. The model calculations are presented in Figure 1 (and Figures S1, S2 in Supplementary

319   data). In this model, particle deposition rate coefficients (k_{dep}) vary with sand size due to the

320   change in the single-collector contact efficiency (η_0). Single-collector contact efficiencies (η_0) for

321   the four different sands at three different CMC-NZVI concentrations (which produced three

322   different d_p) were calculated using the Tufenkji and Elimelech equation (Tufenkji and Elimelech,

323   2004) and are presented in Table 2. Krol et al. (2013) have suggested that reductions in aqueous

324   phase viscosity with time due to dilution (or bypassing) of CMC in the subsurface porous media

325   is responsible for changes in the deposition rate of NZVI over time. In our study, the amount of

326   free CMC available in the solution was very low at approximately 6% (Cirtiu et al., 2011) and

327   much higher doses of dissolved CMC are needed to increase the solution viscosity. Thus the

328   solution viscosity of the CMC-NZVI suspension was taken to be that for water in calculations of

329   the η_0. A value of α_{pc}=0.013 was obtained by fitting Model 1 to the BTC and retention profile

330   corresponding to the lowest CMC-NZVI concentration (0.085 gL^{-1}) in the coarsest sand (775

331   μm). Detachment (k_{det}) of deposited particles for this case was ignored as no tailing in the BTC

332   was observed. Figure 1 shows that the calculated BTC and retention profile for 0.085 gL^{-1} CMC-

333   NZVI (d_p=167 nm) transported through the 775 μm diameter sand fitted well with the

334   experimental data with r^2> 0.99 (Table 2). The fitted value of α_{pc} (0.013) obtained in this study is

335   in the same order of magnitude reported in different studies (0.05-0.072), conducted with similar

336   experimental conditions (Phenrat et al., 2008; Raychoudhury et al., 2012; Saleh et al., 2008). The

337   same value of α_{pc}=0.013 was employed for fitting the model to the data for all other experimental

338   conditions, given the fact that α_{pc} is influenced by aqueous chemistry, which was unchanged in

339   the different experimental systems. The detachment coefficient, k_{det}, was fitted simultaneously to

340   the BTC and retention profiles for the various sand sizes.

341   The fitted BTCs for the coarsest sand (d_c=775 μm) with higher CMC-NZVI concentrations

342   of 0.35 and 1.7 gL^{-1} (d_p=183 nm and 185 nm), compared well with the experimental C/C_0 steady-

343   state values; however, the tailing effect was not captured (Figures S1a, S2a). The best fit values

344   of k_{det} were approximately zero (Table S1), suggesting that the Model 1 is not effective for

345   describing tailing. Furthermore, the measured particle retention near the column inlet was

346   considerably higher compared to Model 1 predictions (Figures S1b, S2b). For sands of smaller

347   diameters (d_c=510 μm, d_c=250 μm and d_c=150 μm), the calculated BTCs, considering the same

348   α_{pc} as the coarser sand, exceed the measured normalized effluent particle concentration and the

349   tailing in the BTC was not captured in the calculations for all of the experimental conditions

350   (Figure 1a, Figures S1a and S2a). Furthermore, for these sands of smaller diameters, the

351 measured particle retention near the column inlet for all CMC-NZVI suspension conditions was

352 very high (Figure 1b and Figures S1b and S2b in Supplementary data), which cannot be

353 explained only by particle deposition,

354   Overall, Model 1, which accounts for particle attachment on different-sized collectors

355 and subsequent detachment, does not adequately account for the BTCs and the retention profiles

356 observed for the three different CMC-NZVI suspensions.

357   A number of studies (Tufenkji and Elimelech, 2004; Tufenkji and Elimelech, 2005)

358 suggest charge heterogeneity on collector surface due to presence of different metal oxide

359 and/hydroxide can lead high particle deposition (at those favorable sites) at the initial stage near

360 the column inlet, which can result in hyper-exponential retention profile. However, in this

361 experiment the sand grains were acid washed to remove all metal oxides and organic content.

362 Thus collector heterogeneity is an unlikely mechanism attributed to high particle retention at the

363 column inlet.

364   Hosseini and Tosco (2013) observed that surface modified bimetallic Fe/Cu nanoparticles

365 were retained extensively at the column inlet during the injection period. However the deposited

366 particles were mobilized along the column length during flushing. In our study, the hyper-

367 exponential particle retention profile even after flushing with several PVs of electrolyte indicates

368 that CMC-NZVI particles were retained at the column inlet in a more stable manner. The

369 discrepancy in the mobility patterns of retained particles along the column length may be

370 attributed the coarser sand of an average diameter of 830 μm and higher concentrations of

371 nanoparticles (of 8 g/L) used by Hosseini and Tosco (2013).

372   An increase in particle retention with decreasing sand size and high particle retention near the

373 column inlet is typically attributed to straining and/or wedging. Therefore, in Model 2, straining

374   of CMC-NZVI was incorporated along with particle deposition and detachment as described

375   earlier.

376

377   **4.3 Model 2: Particle Deposition and Straining**

378   Model 2, which accounts for straining, deposition and detachment of CMC-NZVI was in

379   good agreement ($r^2 > 0.9$) with the experimental BTCs and retention profiles for all experimental

380   scenarios (Figure 2-4). The increasing trend of CMC-NZVI retention in finer sands, particularly

381   near the column inlet was effectively accounted for in Model 2. In general, the tailing in the

382   BTCs was better captured with Model 2. However, for coarsest sand the tailing effect was not

383   perfectly captured, possibly due to other processes occurring in this sand, such as to reversible

384   attachment and detachment of CMC-NZVI (Shang et al., 2010).

385   As with Model 1, the value of $\alpha_{pc}=0.013$ obtained from fitting the BTC and retention

386   profiles for the coarsest sand injected with 0.085 mg/L CMC-NZVI was used for Model 2. For

387   this experimental condition, particle deposition alone can fit the experimental data (Table 2,

388   Figure 1) and the fitted k_{str} value is 0. The fitted values of k_{det} vary within a range of 0.05 to 0.43

389   for all other experimental conditions other than as presented in Table 2. Similar values of

390   detachment rate coefficients relative to the attachment rate coefficients has been reported for

391   studies conducted under unfavourable deposition conditions (Shang et al., 2010; Smith et al.,

392   2008; Tong et al., 2005b) . Our calculations show that although the detachment rate is high, the

393   net deposited mass (S_{dep}) at any location is non-zero over the duration of the experiment.

394   Two fitting parameters are introduced by incorporating straining; namely, the straining

395   rate coefficient (k_{str}), which is dependent on the relative size of particles and sands, and β. A

396   single value of β was fitted for all the experimental conditions to describe the spatial distribution

397   of strained particles over a wide range of colloid and collector sizes. The obtained value of $\beta =$

398   0.609 in this study is in close proximity of that ($\beta = 0.43$) reported elsewhere (Bradford and

399   Bettahar, 2006; Bradford et al., 2003). All parameter values are presented in Table 2. The

400   straining rate coefficients determined in this study vary from 0.09 min^{-1} to 2.15 min^{-1}, and are

401   within the range of previously reported values (Bradford et al., 2003; Tosco and Sethi, 2010; Xu

402   et al., 2006). Bradford et al. (2003) reported a k_{str} value of 0.007 min^{-1} for carboxyl

403   functionalized latex particles of 0.45 μm diameter through Ottawa sand of 150 μm in diameter

404   (d_p/d_c ratio of 0.003). A similar range of k_{str} of 4×10^{-3}-7.9×10^{-3} min^{-1} was reported by Xu et al.

405   (2006) for 0.5 μm latex particles of transported through 98 μm diameter sand with a d_p/d_c ratio of

406   0.0051. We have observed three orders of magnitude higher k_{str} of 1.97 min^{-1} of CMC-NZVI for

407   a similar d_p/d_c ratio of 0.0013. Tosco and Sethi (2010) have reported similarly high straining

408   coefficients in the range of 0.12 to 0.94 min^{-1} for NZVI particles of 70 nm diameter (by TEM),

409   stabilized in xanthan gum suspensions, at a d_p/d_c ratio of 1.01×10^{-4}. For a similar d_p/d_c ratio of

410   2.24×10^{-4} given by the CMC-NZVI of 183 nm size and the 775 μm sand we have estimated a k_{str}

411   of 0.096 min^{-1} in this study. Thus the rate and extent of straining for nanoparticles are higher

412   than those reported by Bradford et al. (2003) and Xu et al. (2006) even at lower d_p/d_c ratios.

413   Tosco and Sethi (2010) have suggested that formation of a large brush layer of xanthan gum

414   around the NZVI might enhance straining of nanoparticles. In this study, straining is observed

415   for a d_p/d_c ratio ranging between 2.24×10^{-4} to 1.23×10^{-3}. Hong et al. (2009) have also

416   demonstrated straining for hematite, magnetite and magnetite/nickel nanoparticles of size 15-50

417   nm with a d_p/d_c ratio range of 5.5×10^{-5}-1.8×10^{-4}. Those authors have suggested formation of

418   aggregates of 400-550 nm in diameter enhance the extent of straining. In our study, similar sized

419   aggregates were present at low concentrations, and may have contributed to straining. In general,

420   latex particles such as those used by Bradford et al. (2003) and Xu et al. (2006), are significantly

421   more mono-disperse than the CMC-NZVI particles used in this study (Figure S3). Thus it is

422   likely that a larger CMC-NZVI aggregate would be strained or wedged at the grain to grain

423   contact point, and additional CMC-NZVI particles would then be retained or attracted to those

424   aggregates (Hong et al., 2009), result in further straining as illustrated in Figure S4. This

425   phenomena are likely responsible for the higher straining coefficient for modified-NZVI

426   particles. The average diameter of pore throats of the different sized sands used in our study are

427   in the range of 58 μm to 302 μm according to the empirical relationship outlined by Bergendahl

428   and Grasso (2000). This suggests that the CMC-NZVI particles were orders of magnitude

429   smaller than the pore throats and yet resulted in significant straining. This is also the case for

430   other studies cited above in this paragraph. It is likely that a larger CMC-NZVI aggregate can

431   initiate straining and/wedging at the pore throat, which can lead to further straining as mentioned

432   above and in the illustration (Figure S4) .The mass of CMC-NZVI retained by straining may

433   alternatively have been retained by wedging between grain to grain contact points. Given that the

434   number of sand grains packed within a unit volume of granular packed media increase with finer

435   sand diameter, the number of grain to grain contact points would also increase with finer sands.

436   Therefore, as with straining, more CMC-NZVI particles are expected to be retained due to

437   wedging with decrease in sand diameter.

438   The change in the straining rate coefficient as a function of the ratio of the mean CMC-

439   NZVI particle hydrodynamic diameter (based on NTA) and the mean sand diameter is presented

440   in Figure 5. The straining rate coefficient shows a linear relationship with the d_p/d_c ratio

441   (r^2=0.97). In this study, the CMC-NZVI particle hydrodynamic diameters fall within a limited

442   range for all transport experiments and the results in Figure 5 suggest that the straining rate

443   coefficient increases linearly with the diameter of the sand grains. Changes in the straining rate

444 coefficient with the d_p/d_c ratio have also been reported elsewhere. Xu et al. (2006) found that the

445 straining rate coefficient varies linearly within a d_p/d_c range of 0.008-0.052, whereas Bradford et

446 al. (2003) reported a power relationship of $(d_p/d_c)^{1.42}$ with the straining rate coefficient.

447

448 **4.4 Spatial distribution of CMC-NZVI in porous media**

449 Our calculations suggest that retained mass in the sand packed column is governed

450 primarily by straining. To demonstrate this, the percentage of strained mass relative to the total

451 injected CMC-NZVI at the inlet (within 2 cm of column length) and beyond was calculated

452 using Model 2. The mass percentage at the column inlet was denoted by $M_{str,L=0-2}$ and beyond this

453 point it was denoted by $M_{str,L=2-9}$ (Table 2). The data presented in Table 2 shows that with

454 decreasing sand size, the percentage of strained mass increases steadily. It is interesting to note

455 that the percentage of strained mass reduces after 2 cm of column length for all sand sizes and

456 concentrations. Within the first 2 cm of the inlet, approximately 19% of the CMC-NZVI mass

457 injected was retained due to straining with the finest sand and 0.35 gL^{-1} CMC-NZVI. In the

458 remaining 7 cm of the column, only an additional 21% was retained by straining. Similarly,

459 approximately half of the CMC-NZVI was retained within 2 cm of column length for the other

460 sand sizes and CMC-NZVI concentrations.

461 High particle retention due to straining at the column inlet could result in changes in

462 porosity, permeability and eventually in the flow rate. Hosseini and Tosco (2013) have

463 demonstrated that an increase in pressure drop over time resulted from pore clogging during

464 injection of modified Fe/Cu nanoparticle at high concentrations of 5-12 g/L. Several studies have

465 reported that polymer-stabilized NZVI, when injected in the field at g/L concentrations, are

466 retained within few centimeters to 2.1 m to from the point of injection (He et al., 2010; Johnson

467 et al., 2013; Su et al., 2013). Furthermore, NZVI particles may be transformed into micron-sized

468 aggregates in natural systems (Johnson et al., 2013; Su et al., 2013). Thus straining would be

469 even more prevalent under field scenarios.

470

471 **5. Conclusion**

472   In this study, the significance of straining as a retention mechanism during the transport of

473 a polyelectrolyte-stabilized NZVI particle was investigated systematically for the first time. The

474 results demonstrate that straining can be an important retention mechanism for the transport of

475 polymer-stabilized NZVI in granular porous media. There was a higher extent of CMC-NZVI

476 retention, primarily due to straining, in finer sands (150 and 250 μm diameter) than in coarser

477 sands (510 and 775 μm diameter). A change in the CMC-NZVI influent concentration from

478 0.085 to 1.7 g/L had little impact on the mass of CMC-NZVI retained by straining.

479 Approximately 50% of the total retained mass of CMC-NZVI was present in the first 2 cm of the

480 column inlet due to straining. It should be noted that physicochemical deposition also contributed

481 to particle retention, however, a fraction of the CMC-NZVI mass deposited was subsequently

482 released back into the pore fluid. The numerical model incorporating particle deposition,

483 detachment and straining exhibited a significantly better fit to the BTCs and retention profiles,

484 compared to the model that did not account for straining. The values of the deposition,

485 detachment and straining rate coefficients obtained from fitting of the model to experimental

486 data, were in the range of values reported in other studies. Although polyelectrolyte or polymer

487 coatings can significantly improve NZVI mobility in granular porous media, our results suggest

488 that with finer sands there will be significant retention of CMC-NZVI closer to the point of

489 injection due to straining. Such spatial distributions of particle retention need to be accounted for

490 in delivering target doses of NZVI to various locations in contaminated aquifers. It should be

491 noted however, that the ionic strength of 0.1 mM for the electrolyte medium used in this study is

492 lower than that typically encountered in groundwaters. At higher groundwater ionic strengths,

493 enhanced aggregation and particle deposition (Raychoudhury et al., 2012; Saleh et al., 2008)

494 would intensify straining.

495

501
502 **Supporting Information Available**

503   Supporting information provides fitted parameters for Model 1, experimental and predicted

504 BTCs and retention profiles for CMC-NZVI of concentrations 0.35 gL^{-1} and 1.7 gL^{-1} (Model 1).

505

506   **Literature Cited**

507 Bergendahl, J., Grasso, D., 2000. Prediction of colloid detachment in a model porous media:
508   Hydrodynamics. *Chemical Engineering Science*. 55, 1523-1532.
509 Bradford, S. A., Bettahar, M., 2006. Concentration dependent transport of colloids in saturated
510   porous media. *Journal of Contaminant Hydrology*. 82, 99-117.
511 Bradford, S. A., Simunek, J., Bettahar, M., Van Genuchten, M. T., Yates, S. R., 2003. Modeling
512   colloid attachment, straining, and exclusion in saturated porous media. *Environmental
513   Science and Technology*. 37, 2242-2250.
514 Cirtiu, M. C., Raychoudhury, T., Ghoshal, S., Moores, A., 2011. Systematic Comparison of the
515   Size, Surface Characteristics and Colloidal Stability of Zero Valent Iron Nanoparticles
516   Preand Post-Grafted with Common Polymers. *Colloids and Surfaces A: Physicochemical
517   Engineering Aspects*. 390, 95-104.
518 Fatisson, J., Ghoshal, S., Tufenkji, N., 2010. Deposition of carboxymethylcellulose-coated zero-
519   valent iron nanoparticles onto silica: Roles of solution chemistry and organic molecules.
520   *Langmuir*. 26 (15), 12832-12840.

He, F., Zhang, M., Qian, T., Zhao, D., 2009. Transport of carboxymethyl cellulose stabilized iron nanoparticles in porous media: Column experiments and modeling. *Journal of Colloid and Interface Science*. 334 (1), 96-102.

He, F., Zhao, D., 2007. Manipulating the size and dispersibility of zerovalent iron nanoparticles by use of carboxymethyl cellulose stabilizers. *Environmental Science and Technology*. 41 (17), 6216-6221.

He, F., Zhao, D., Paul, C., 2010. Field assessment of carboxymethyl cellulose stabilized iron nanoparticles for in situ destruction of chlorinated solvents in source zones. *Water Research*. 44 (7), 2360-2370.

Hong, Y., Honda, R. J., Myung, N. V., Walker, S. L., 2009. Transport of iron-based nanoparticles: Role of magnetic properties. *Environmental Science and Technology*. 43, 8834-8839.

Hosseini, S. M., Tosco, T., 2013. Transport and retention of high concentrated nano-Fe/Cu particles through highly flow-rated packed sand column. *Water Research*. 47 (1), 326-338.

Jaisi, D. P., Elimelech, M., 2009. Single-walled carbon nanotubes exhibit limited transport in soil columns. *Environmental Science and Technology*. 43, 9161-9166.

Johnson, R. L., Nurmi, J. T., Johnson, G. S. O., Fan, D. M., Johnson, R. L. O., Shi, Z. Q., Salter-Blanc, A. J., Tratnyek, P. G., Lowry, G. V., 2013. Field-Scale Transport and Transformation of Carboxymethylcellulose-Stabilized Nano Zero-Valent Iron. *Environmental Science and Technology*. 47 (3), 1573-1580.

Krol, M. M., Oleniuk, A. J., Kocur, C. M., Sleep, B. E., Bennett, P., Xiong, Z., O'Carroll, D. M., 2013. A Field-Validated Model for In Situ Transport of Polymer-Stabilized nZVI and Implications for Subsurface Injection. *Environmental Science and Technology*. 47 (13), 7332–7340.

Kuhnen, F., Barmettler, K., Bhattacharjee, S., Elimelech, M., Kretzschmar, R., 2000. Transport of iron oxide colloids in packed quartz sand media: Monolayer and multilayer deposition. *Journal of Colloid and Interface Science*. 231 (1), 32-41.

Li, X., Zhang, P., Lin, C. L., Johnson, W. P., 2005. Role of hydrodynamic drag on microsphere deposition and re-entrainment in porous media under unfavorable conditions. *Environmental Science and Technology*. 39, 4012-4020.

Marquardt, D. W., 1963. An algorithm for least-squares estimation of nonlinear parameters. *Journal of the Society for Industrial and Applied Mathematics*. 11 (2), 431-441.

Mueller, N. C., Braun, J., Bruns, J., Černík, M., Rissing, P., Rickerby, D., Nowack, B., 2012. Application of nanoscale zero valent iron (NZVI) for groundwater remediation in Europe. *Environment Science and Pollution Research*. 19, 550–558.

O'Carroll, D., Sleep, B., Krol, M., Boparai, H., Kocur, C., 2012. Nanoscale zero valent iron and bimetallic particles for contaminated site remediation. *Advances in Water Resources*. 51, 104-122.

Petosa, A. R., Jaisi, D. P., Quevedo, I. R., Elimelech, M., Tufenkji, N., 2010. Aggregation and deposition of engineered nanomaterials in aquatic environments: Role of physicochemical interactions. *Environmental Science and Technology*. 44 (17), 6532-6549.

Phenrat, T., Kim, H.-J., Fagerlund, F., Illangasekare, T., Lowry, G. V., 2010. Empirical correlations to estimate agglomerate size and deposition during injection of a

polyelectrolyte-modified Fe0 nanoparticle at high particle concentration in saturated sand. *Journal of Contaminant Hydrology*. 118 (3-4), 152-164.

Phenrat, T., Kim, H.-J., Fagerlund, F., Illangasekare, T., Tilton, R. D., Lowry, G. V., 2009. Particle size distribution, concentration, and magnetic attraction affect transport of polymer-modified Fe0 nanoparticles in sand columns. *Environmental Science and Technology*. 43 (13), 5079-5085.

Phenrat, T., Saleh, N., Sirk, K., Kim, H.-J., Tilton, R. D., Lowry, G. V., 2008. Stabilization of aqueous nanoscale zerovalent iron dispersions by anionic polyelectrolytes: Adsorbed anionic polyelectrolyte layer properties and their effect on aggregation and sedimentation. *Journal of Nanoparticle Research*. 10 (5), 795-814.

Raychoudhury, T., Naja, G., Ghoshal, S., 2010. Assessment of transport of two polyelectrolyte-stabilized zero-valent iron nanoparticles in porous media. *Journal of Contaminant Hydrology*. 118, 143-151.

Raychoudhury, T., Tufenkji, N., Ghoshal, S., 2012. Aggregation and deposition kinetics of carboxymethyl cellulose-modified zero-valent iron nanoparticles in porous media. *Water Research*. 46 (6), 1735-1744.

Redman, J. A., Walker, S. L., Elimelech, M., 2004. Bacterial Adhesion and Transport in Porous Media: Role of the Secondary Energy Minimum. *Environmental Science and Technology*. 38, 1777-1785.

Saleh, N., Kim, H.-J., Phenrat, T., Matyjaszewski, K., Tilton, R. D., Lowry, G. V., 2008. Ionic strength and composition affect the mobility of surface-modified fe0 nanoparticles in water-saturated sand columns. *Environmental Science and Technology*. 42 (9), 3349-3355.

Shang, J. Y., Liu, C. X., Wang, Z. M., Wu, H., Zhu, K. K., Li, J. A., Liu, J., 2010. In-Situ Measurements of Engineered Nanoporous Particle Transport in Saturated Porous Media. *Environmental Science and Technology*. 44 (21), 8190-8195.

Smith, J., Gao, B., Funabashi, H., Tran, T. N., Luo, D., Ahner, B. A., Steenhuis, T. S., Hay, A. G., Walter, M. T., 2008. Pore-scale quantification of colloid transport in saturated porous media. *Environmental Science and Technology*. 42 (2), 517-523.

Su, C. M., Puls, R. W., Krug, T. A., Watling, M. T., O'Hara, S. K., Quinn, J. W., Ruiz, N. E., 2013. Travel distance and transformation of injected emulsified zerovalent iron nanoparticles in the subsurface during two and half years. *Water Research*. 47 (12), 4095-4106.

Tong, M., Li, X., Brow, C. N., Johnson, W. P., 2005a. Detachment-influenced transport of an adhesion-deficient bacterial strain within water-reactive porous media. *Environmental Science and Technology*. 39, 2500-2508.

Tong, M. P., Camesano, T. A., Johnson, W. P., 2005b. Spatial variation in deposition rate coefficients of an adhesion-deficient bacterial strain in quartz sand. *Environmental Science and Technology*. 39 (10), 3679-3687.

Torkzaban, S., Bradford, S. A., Walker, S. L., 2007. Resolving the coupled effects of hydrodynamics and DLVO forces on colloid attachment in porous media. *Langmuir*. 23 (19), 9652-9660.

Torkzaban, S., Kim, Y., Mulvihill, M., Wan, J., Tokunaga, T. K., 2010. Transport and deposition of functionalized CdTe nanoparticles in saturated porous media. *Journal of Contaminant Hydrology*. 118, 208-217.

Tosco, T., Sethi, R., 2010. Transport of non-newtonian suspensions of highly concentrated micro- and nanoscale iron particles in porous media: A modeling approach. *Environmental Science and Technology*. 44, 9062-9068.

Tufenkji, N., Elimelech, M., 2004. Correlation Equation for Predicting Single-Collector Efficiency in Physicochemical Filtration in Saturated Porous Media. *Environmental Science and Technology*. 38, 529-536.

Tufenkji, N., Elimelech, M., 2005. Breakdown of colloid filtration theory: Role of the secondary energy minimum and surface charge heterogeneities. *Langmuir*. 21 (3), 841-852.

Tufenkji, N., Miller, G. F., Ryan, J. N., Harvey, R. W., Elimelech, M., 2004. Transport of Cryptosporidium oocysts in porous media: Role of straining and physicochemical filtration. *Environmental Science and Technology*. 38, 5932-5938.

Xu, S., Gao, B., Saiers, J. E., 2006. Straining of colloidal particles in saturated porous media. *Water Resources Research*. 42 (W12S16), doi:10.1029/2006WR004948.

Yao, K. M., Habibian, M. T., O'Melia, C. R., 1971. Water and waste water filtration:Concepts and applications. *Environmental Science and Technology*. 5 (11), 1105-1112.

Zhang, W.-X., 2003. Nanoscale iron particles for environmental remediation: An overview. *Journal of Nanoparticle Research*. 5, 323-333.

LIST OF FIGURES

FIGURE 1: Experimental and calculated (a) breakthrough curves and (b) retention profiles along the column length of CMC-NZVI with $C_0 = 0.085$ gL^{-1} in columns of different sized sands. Calculated breakthrough curves and retention profiles shown with lines were obtained using Model 1.

FIGURE 2: Experimental and calculated (a) breakthrough curves and (b) retention profiles along the column length of CMC-NZVI with $C_0 = 0.085$ gL^{-1} in columns of different sized sands. Calculated breakthrough curves and retention profiles shown with lines were obtained by fitting Model 2.

FIGURE 3: Experimental and calculated (a) breakthrough curves and (b) retention profiles along the column length of CMC-NZVI with $C_0 = 0.35$ gL^{-1} in columns of different sized sands. Calculated breakthrough curves and retention profiles shown with lines were obtained by fitting Model 2.

FIGURE 4: Experimental and simulated (a) breakthrough curves and (b) retention profiles along the column length of CMC-NZVI with $C_0 = 1.70$ gL^{-1} in columns of different sized sands. Calculated breakthrough curves and retention profiles shown with lines were obtained by fitting Model 2.

FIGURE 5: Fitted straining rate coefficient (k_{str}) obtained using Model 2, varies linearly with d_p/d_c ratio. d_p is the mean hydrodynamic diameter of CMC-NZVI and d_c is the mean sand grain diameter.

Table 1: Experimental conditions and parameters for column experiments

Column length, L	9 cm
Nano iron concentration of the column feed, C_0	0.085, 0.35 or 1.7 gL^{-1}
Darcy velocity, U	0.445 cmmin^{-1}
Packing density of dry sand in the packed-bed, ρ_b	1.95 g cm^{-3}
Density of the nanoparticles	6.7×10^3 kgm^{-3}
pH of the CMC-NZVI suspension	7.4±0.4
Ionic strength of electrolyte solution as prepared	0.1 mM of NaHCO$_3$
Dispersion coefficient, D	0.13 cm^{2}min^{-1} (775-150 μm sand grains)
Porosity, ε	0.35 (for 775 μm dia sand), 0.32 (510-150 μm dia sands)

Table 2: Column transport experiment results and estimated parameters at different experimental conditions

Sand grade	d_c (µm)	d_p (NTA)	C_0 (g/L)	C/C_0	η_0	$M_{balance}$ (%)	k_{dep} (min⁻¹)	k_{det} (min⁻¹)	k_{str} (min⁻¹)	$M_{str,L=0-2}$ (%)	$M_{str,L=2-9}$ (%)	$^a r_{C/C_0}^2$	$^b r_S^2$
F2025	775	167	0.085	0.95	0.0173	88.5	0.0036	0	0	0	0	0.99	1.00
	775	183	0.35	0.97	0.0164	92.5	0.0034	0.16	0.096	3.03	4.36	0.94	0.99
	775	185	1.7	0.89	0.0163	94.8	0.0034	0.16	0.096	3.03	4.36	0.97	0.99
F3040	510	167	0.085	0.84	0.0222	98	0.0080	0.09	0.33	7.14	9.55	0.98	0.82
	510	183	0.35	0.82	0.0209	95.5	0.0076	0.09	0.40	8.52	11.21	0.93	0.95
	510	185	1.7	0.77	0.0208	97.6	0.0075	0.09	0.40	8.52	11.21	0.95	0.85
F5070	250	167	0.085	0.57	0.0344	98.9	0.0254	0.05	1.13	17.25	19.49	0.92	0.96
	250	183	0.35	0.67	0.0322	95.5	0.0238	0.05	1.00	13.71	16.22	0.90	0.99
	250	185	1.7	0.6	0.0319	92	0.0235	0.05	1.00	13.70	16.23	0.96	0.99
F70140	150	167	0.085	0.55	0.0473	92.8	0.0581	0.43	2.15	20.30	22.39	0.96	0.99
	150	183	0.35	0.62	0.0442	92.7	0.0543	0.43	1.97	18.82	21.17	0.92	0.99
	150	185	1.7	0.6	0.0439	86.7	0.0540	0.43	1.97	18.82	21.17	0.93	0.99

Note:

$^a r_{C/C0}^2 = r^2$ value for fitted model values and experimental data points for breakthrough curves

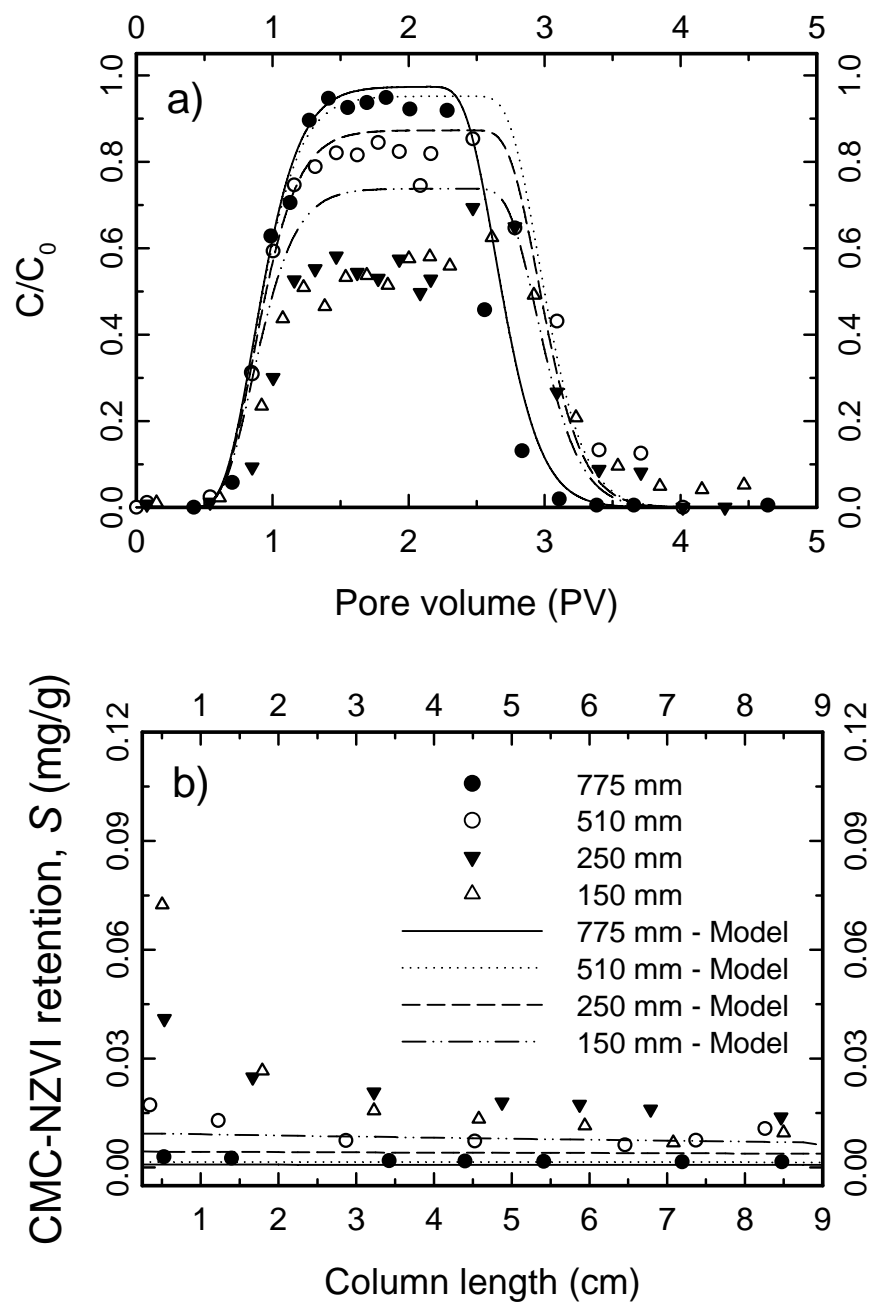$^b r_s^2 = r^2$ value for fitted model values and experimental data points for retention profile along the column length
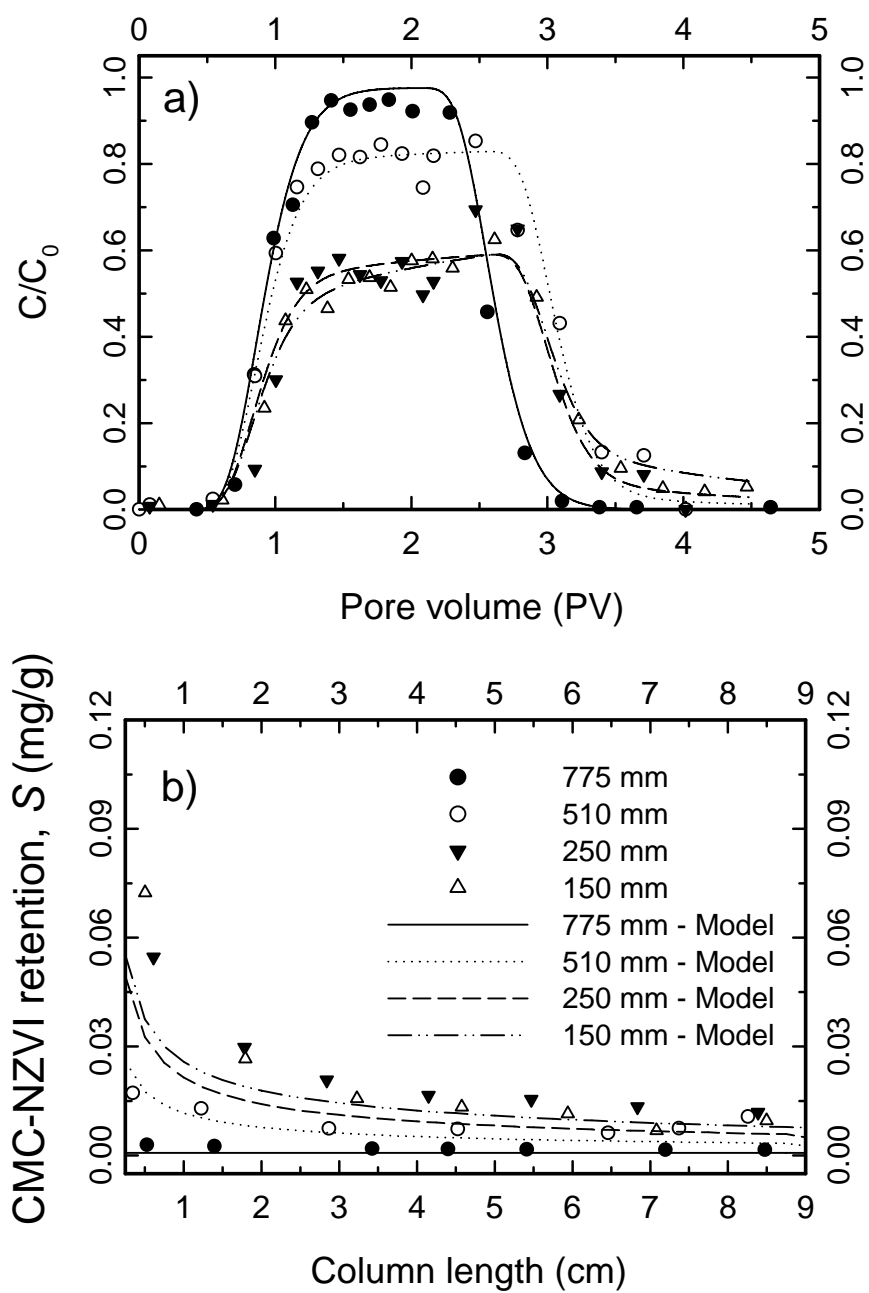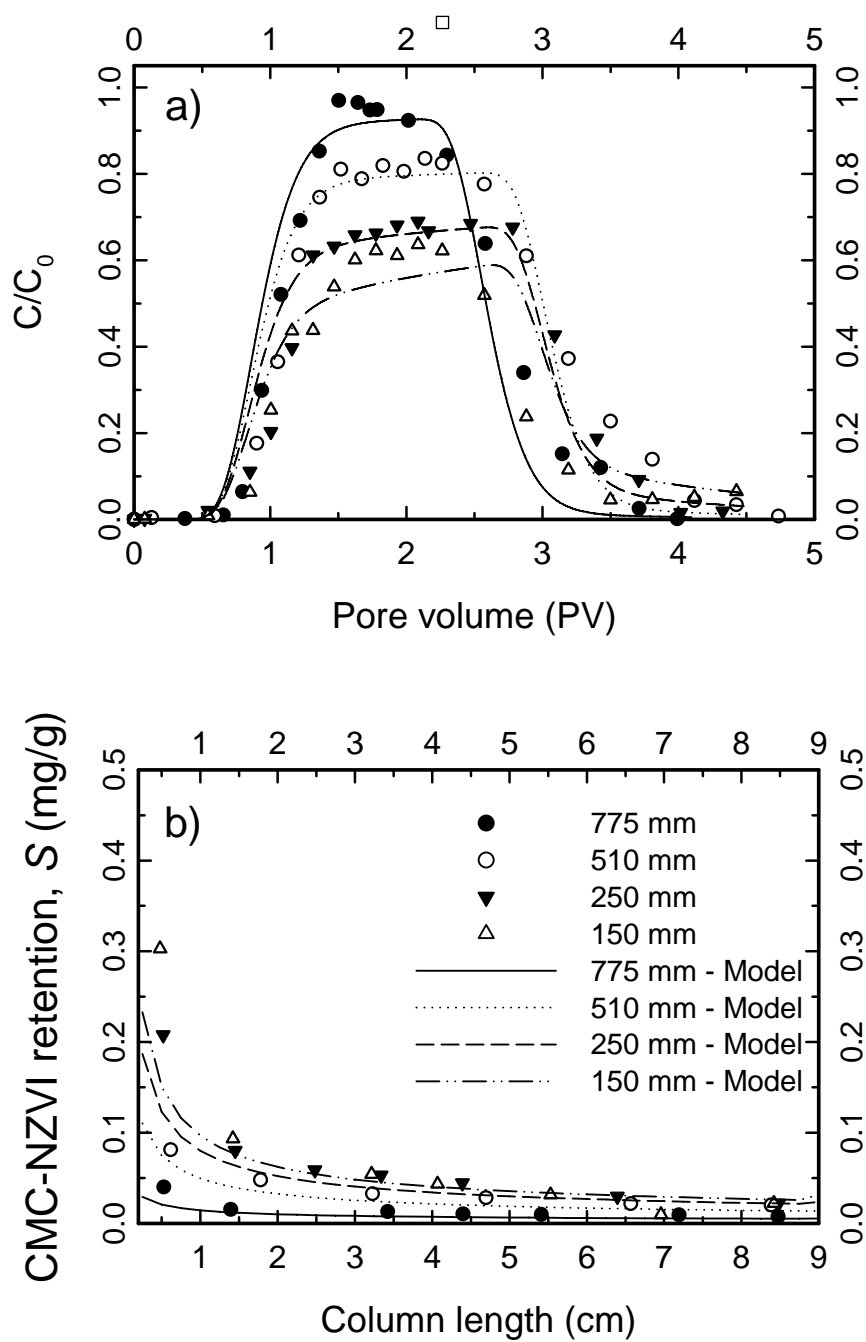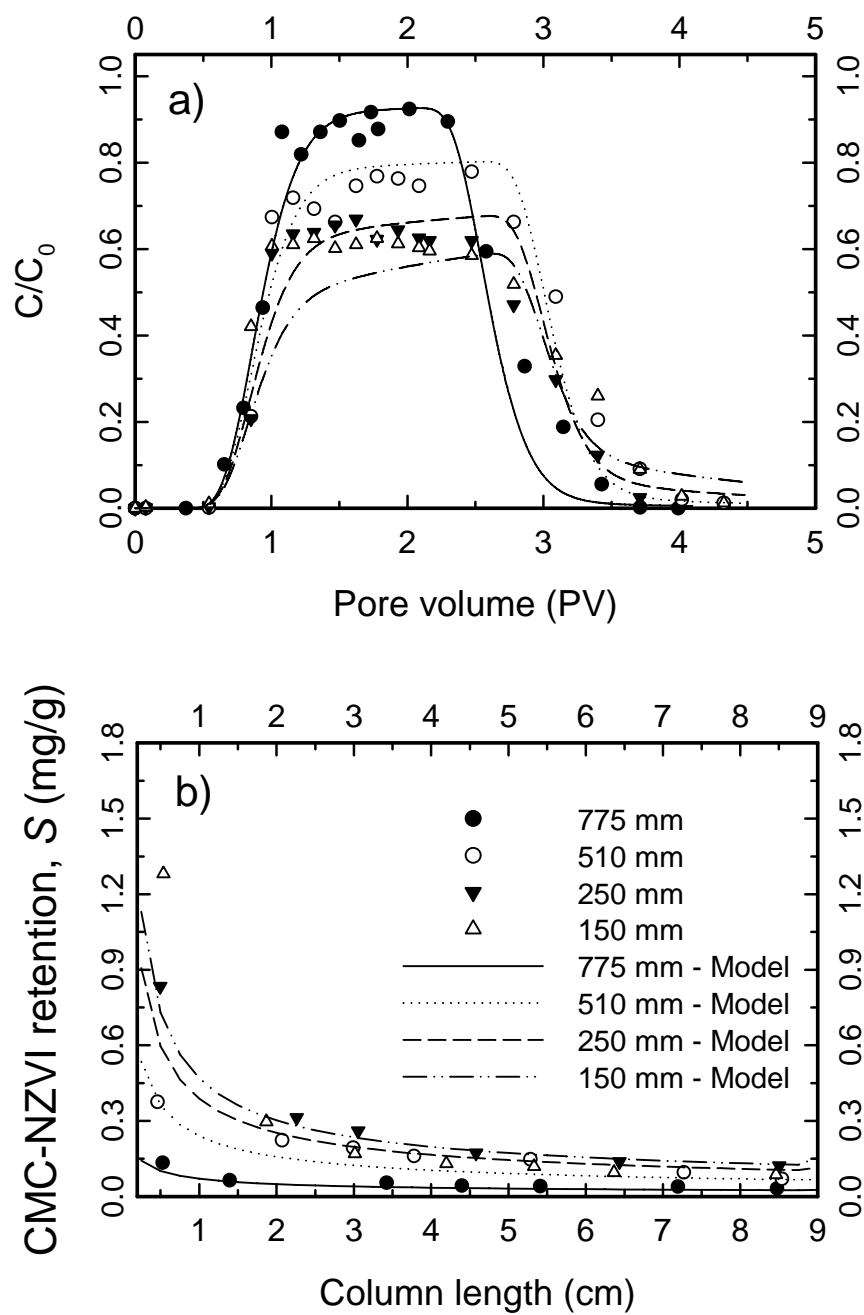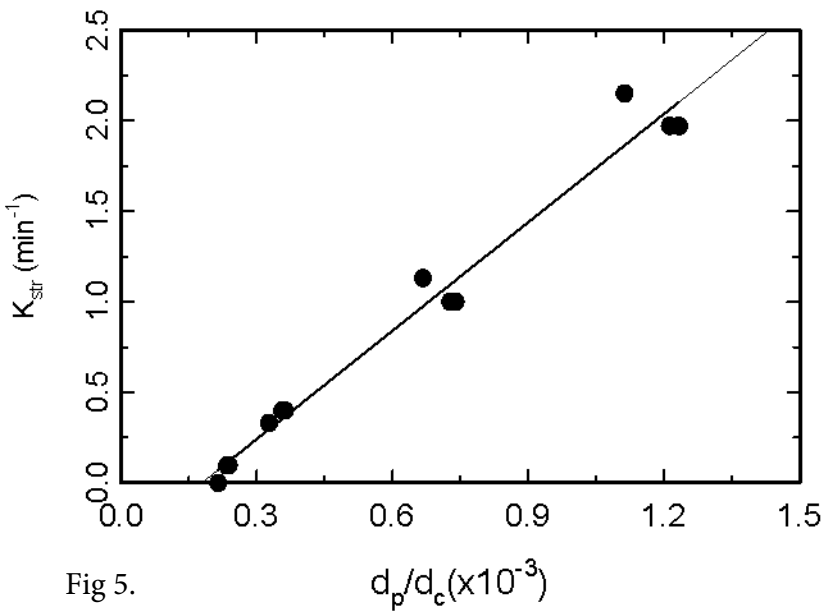
Figure 1.

Figure 2.

Figure 3.

Figure 4.

Fig 5.

Supporting data

Straining of Polyelectrolyte-Stabilized Nanoscale Zero Valent Iron Particles during Transport through Granular Porous Media

Trishikhi Raychoudhury[1,3], Nathalie Tufenkji[2], Subhasis Ghoshal[1,]*

[1] Department of Civil Engineering, McGill University, Montreal, Quebec, Canada H3A 2K6

[2] Department of Chemical Engineering, McGill University, Montreal, Quebec, Canada H3A 2B2

[3] Current address: Department of Applied Geosciences, Technische Universität Berlin, 10587, Berlin, Germany

Table S1: Estimated parameters at different experimental condition incorporating deposition and detachment-Model 1 (with α_{pc}=0.013).

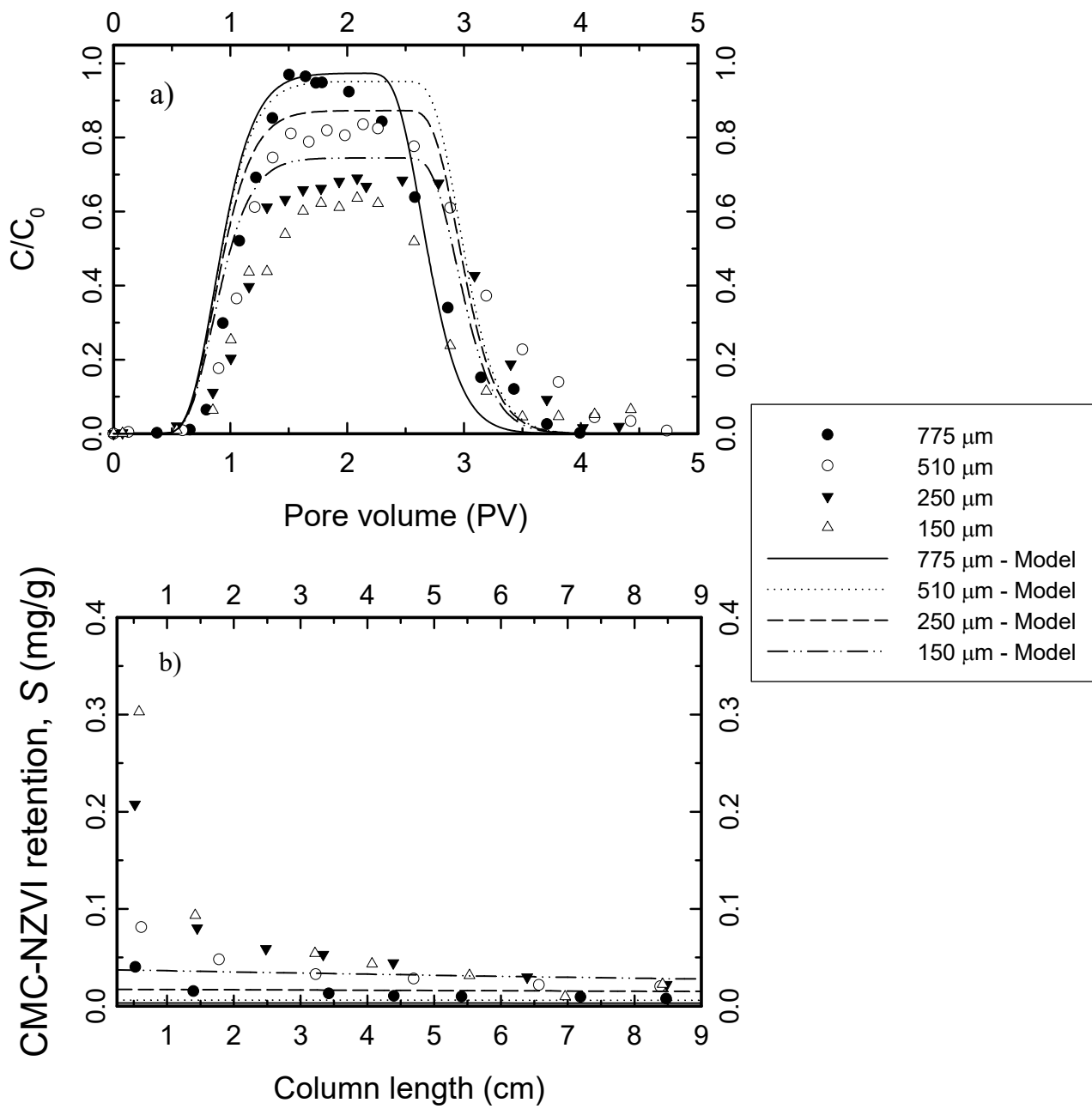| Sand	d_c (μm)	C_0 (g/L)	C/C_0	k_{dep} (min^{-1})	k_{det} (min^{-1})
F2025	775	0.085	0.95	0.0036	0
	775	0.35	0.97	0.0034	0.0043
	775	1.7	0.89	0.0034	0.0043
F3040	510	0.085	0.84	0.0080	0
	510	0.35	0.82	0.0076	0
	510	1.7	0.77	0.0075	0
F5070	250	0.085	0.57	0.0254	0
	250	0.35	0.67	0.0238	0
	250	1.7	0.6	0.0235	0
F70140	150	0.085	0.55	0.0581	0
	150	0.35	0.62	0.0543	0
	150	1.7	0.6	0.0540	0

FIGURE S1: Experimental and calculated (a) breakthrough curves and (b) retention profiles along the column length of CMC-NZVI with C_0 = 0.35 gL^{-1} in columns of different sized sands. Calculated breakthrough curves and retention profiles shown with lines were obtained using Model 1.
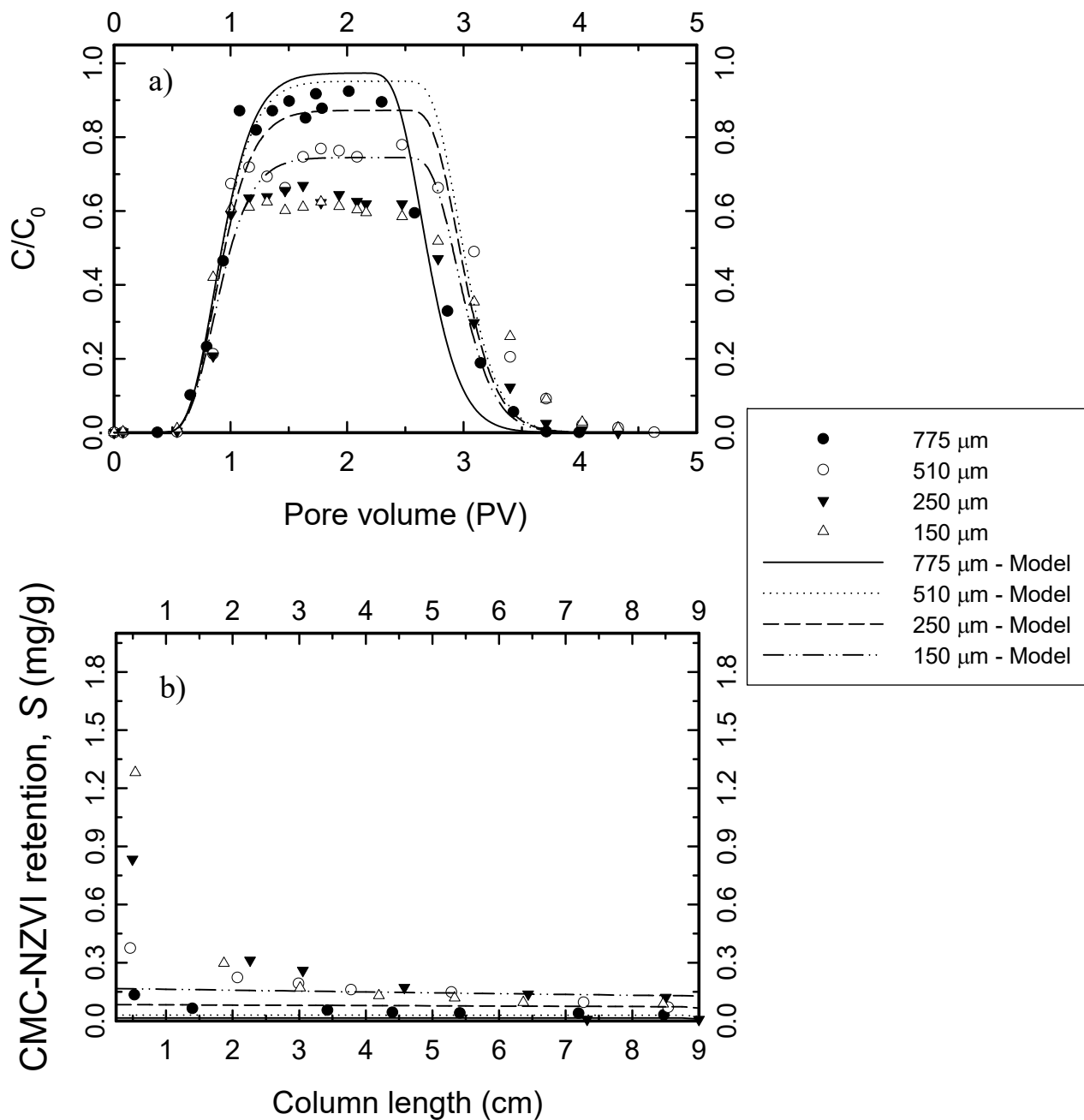
FIGURE S2: Experimental and calculated (a) breakthrough curves and (b) retention profiles along the column length of CMC-NZVI with C_0 = 1.70 gL^{-1} in columns of different sized sands. Calculated breakthrough curves and retention profiles shown with lines were obtained using Model 1.
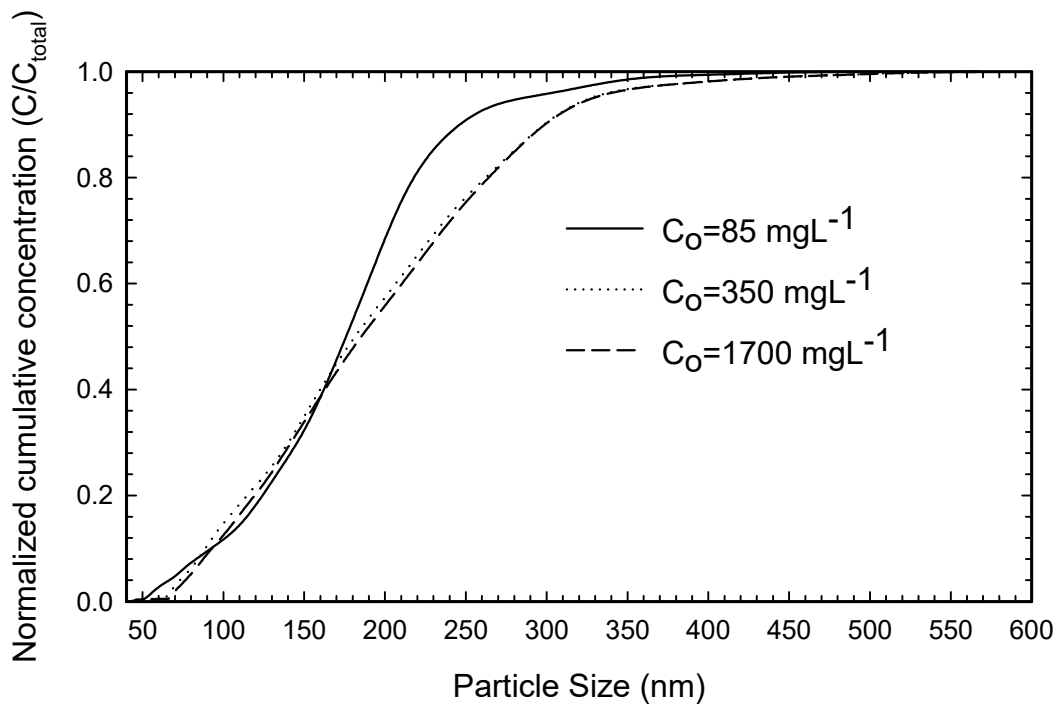
FIGURE S3: Cumulative particle size distribution for three different concentrations (C_0 = 0.085, 0.35 and 1.70 gL^{-1}) measured by Nanoparticle Tracking Analysis (NTA).
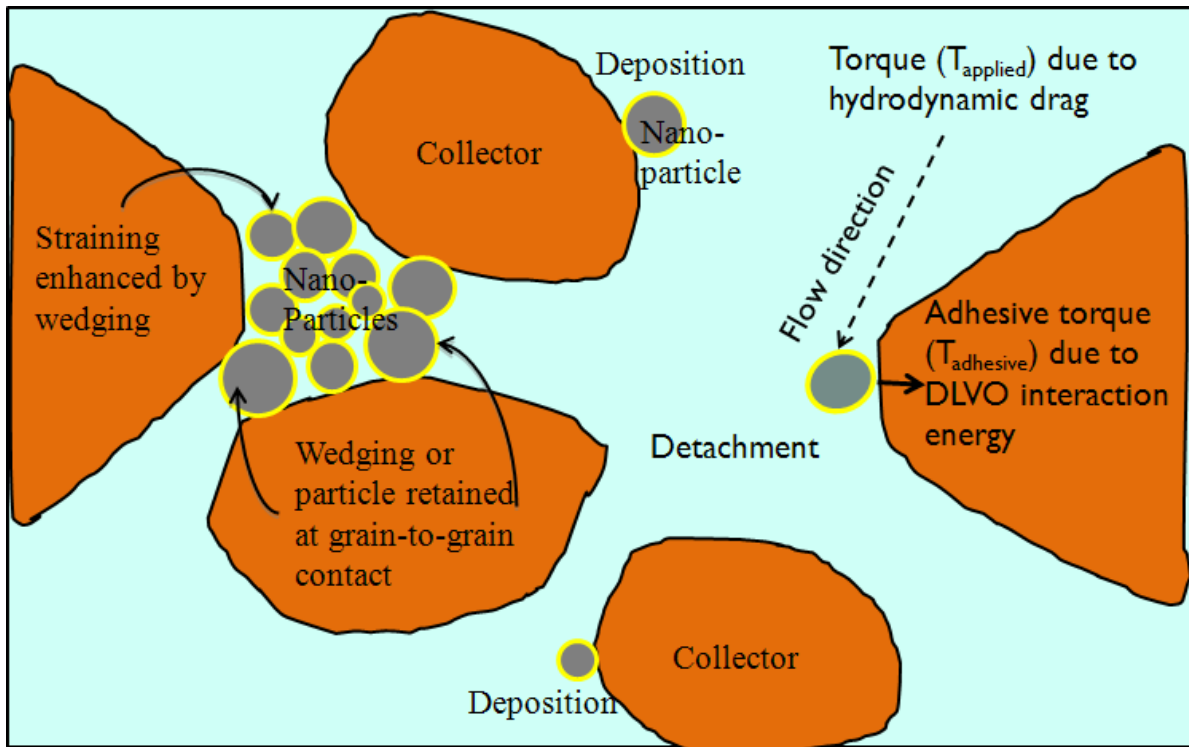

FIGURE S4: Schematic of particle transport in a porous media, indicating particle deposition, detachment and straining.